

Classicality from quantumness revealed by disturbance-free measurement

Sang Min Lee^{1,2,*}, Minsu Kim¹, Heonoh Kim¹, Han Seb Moon^{1,†} and Sang Wook Kim^{3‡}

¹*Department of Physics, Pusan National University, Busan 46241, South Korea*

²*Korea Research Institute of Standards and Science, Daejeon 34113, South Korea and*

³*Department of Physics Education, Pusan National University, Busan 46241, South Korea*

(Dated: October 11, 2017)

We propose an asymptotic disturbance-free measurement using the so-called weak-value scheme, where the weakly measured quantum system is measured for a second time, to confirm that it is disturbance-free; moreover, the probability of obtaining the non-disturbed state must approach one. We show that the weak-measurement outcomes of the Bell state post-selected in this manner exhibit classical behavior in the sense that they satisfy the Clauser-Horne-Shimony-Holt inequality. However, the inequality is violated if all outcomes without post-selection are considered. We experimentally confirm our idea by performing joint weak measurement of polarization-entangled photon-pairs and subsequent fiber-based Bell-state measurement.

One of the strange features of quantum mechanics is the inevitable measurement-induced disturbance, which manifests in the original description of Heisenberg’s uncertainty principle [1–3], although its interpretation remains under debate [4, 5]. Feynman demonstrated, in his well-known book, that measurement-induced photon momentum transfer, in the spirit of the uncertainty principle, is sufficient to eliminate the interference fringes in electron double-slit interferometry [6]. We now know that, even without momentum transfer, we obtain sufficient information to cause complete decoherence [7]; this information is important from a quantum mechanical perspective. The so-called “quantum non-demolition measurement” also disturbs the measured system, in the sense that the quantity canonically conjugated to the measured observable is disturbed, although the measured observable itself is not [8]. Generally speaking, measurement and information gathering disturb and alter the state of the measured system, from the initial pure state $|\psi_i\rangle$ to a final density matrix ρ [9–15]. We often define the infidelity, which quantifies the degree of disturbance of $|\psi_i\rangle$, as [9]

$$D \equiv 1 - \langle \psi_i | \rho | \psi_i \rangle. \quad (1)$$

In contrast, in classical mechanics, one can obtain information from a system without disturbing it. The measurement outcome directly reflects the property that the observed system has already owned before measurement, which guarantees the so-called “realism” of classical mechanics. In this paper, we pose the following question: If we gather information from a *quantum* system *without* disturbing it, does the outcome exhibit *classical* behavior? Two subtle problems exist: (i) A disturbance-free measurement method and (ii) a classical behavior identification scheme are both required.

As regards the first issue, one naive approach to obtaining information from a quantum system without disturbance is to measure the system very weakly. We emphasize that, regardless of the degree of measurement “weakness”, the measured state is disturbed [15]. There-

fore, a non-zero probability that the measured state will be found orthogonal to the original state always exists. Thus, the weak-measurement condition is insufficient to achieve disturbance-free measurement.

Our novel approach to realizing disturbance-free measurement is as follows (see also, Fig. 1). First, we *very weakly* measure an observable M of a system in state $|\psi_i\rangle$. We obtain the outcome m , and the state is changed to ρ . In general, $|\psi_i\rangle$ is not an eigenstate of M . We then perform projection measurement on ρ . If and only if ρ is collapsed to $|\psi_i\rangle$, the outcomes of the weak measurement are selected and labelled m^* . If the weak measurement is truly sufficiently weak to meet requirements, the majority of the outcomes are selected, as ρ does not differ significantly from $|\psi_i\rangle$. This is guaranteed from the fact that the disturbance D goes to zero in the weak measurement limit ([16], Sec. I). We can state with confidence that each selected outcome m^* is information obtained without disturbing the system, as m^* is only recorded if we confirm nondisturbance of the state. The average of such conditional outcomes of weak measurement over

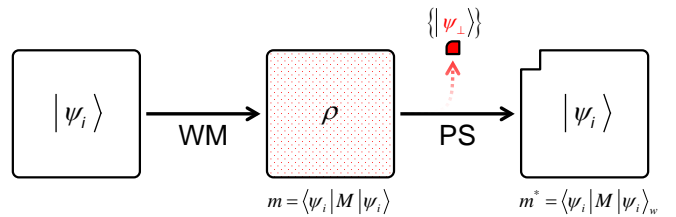


FIG. 1. Schematic diagram of disturbance-free measurement (DFM). An observable M of the initial state $|\psi_i\rangle$ is very weakly measured, so as to be infinitesimally modified to ρ . The average of the measured outputs is equivalent to the quantum mechanical average, $m = \langle \psi_i | M | \psi_i \rangle$. DFM is achieved when the average of the M outcomes post-selected onto the initial state $|\psi_i\rangle$ only are considered, $m^* = \langle \psi_i | M | \psi_i \rangle_w$; this simply corresponds to the so-called “weak-value scheme”. The outcomes of the post-selection are mostly $|\psi_i\rangle$ with a tiny portion of $\{|\psi_\perp\rangle\}$, the subset orthogonal to $|\psi_i\rangle$. WM: weak measurement; PS: post-selection.

the post-selected data is called the *weak value* [17], $\langle M \rangle_w$. Note that, if we average over all m ignoring the results of the final projection measurement, we simply retrieve the quantum mechanical average $\langle M \rangle$. This is because the distribution of m of weak measurement is gaussian with large width due to weak measurement but with the center equivalent to the quantum mechanical average ([16], Sec. II).

The second problem is subtler. A large number of studies have examined approaches to obtaining classicality from quantumness [18–21]. Here, we exploit the Clauser-Horne-Shimony-Holt (CHSH) inequality [22] to determine whether the outcomes behave classically. The CHSH inequality reads

$$|S| = |C(A, B) + C(A, B') + C(A', B) - C(A', B')| \leq 2, \quad (2)$$

where C denotes the correlation between two observables A (or A') and B (or B'). With the Bell state $|S\rangle$ maximally violates this inequality to reach $2\sqrt{2}$, and such an inequality violation unambiguously exhibits quantumness. We obtain the S of an arbitrary pure state $|\psi\rangle$ from the disturbance-free measurement, as explained above, where

$$S_{\text{DFM}} = \langle \psi | AB | \psi \rangle_{\text{DFM}} + \langle \psi | AB' | \psi \rangle_{\text{DFM}} + \langle \psi | A'B | \psi \rangle_{\text{DFM}} - \langle \psi | A'B' | \psi \rangle_{\text{DFM}}. \quad (3)$$

Here, we must define the so-called ‘‘joint weak values’’ [23], i.e., the weak values of two observables ([16], Sec. III). If we introduce the coupling strength s between the measured system and the measurement device [24, 25], we can show that $|S_{\text{DFM}}| \leq 2$ for an arbitrary two-qubit state (including maximally entangled states) $|\psi\rangle$ in the weak measurement limit $s \rightarrow 0$ ([16], Sec. IV). Simultaneously, the probability of obtaining $|\psi\rangle$ in the final projection measurement approaches 1. These two conditions guarantee that S_{DFM} is only averaged over the measurement outcomes obtained without disturbing the state. Thus, our main query is answered in the affirmative, i.e., if we gather information from a quantum system without disturbance, the outcome exhibits classical behavior. Note that the classicality revealed by our DFM can be described by the local hidden variable model ([16], Sec. V). Note also that, with only a single observable at different times, one can also identify classicality using different criteria, for example, the Leggett-Garg inequality [26]. However, we demonstrate that a trivial result is obtained ([16], Sec. VI).

In real experiments, it is difficult to realize the weak measurement limit $s \rightarrow 0$. Thus, we perform experiments as a function of s with the singlet state (one of the Bell states). We expect that $|S|$, beginning with a value larger than the classical bound 2, decreases and moves below this bound as $s \rightarrow 0$. For arbitrary s , $|S|$ can be calculated using our theory ([16], Sec. III). Although our

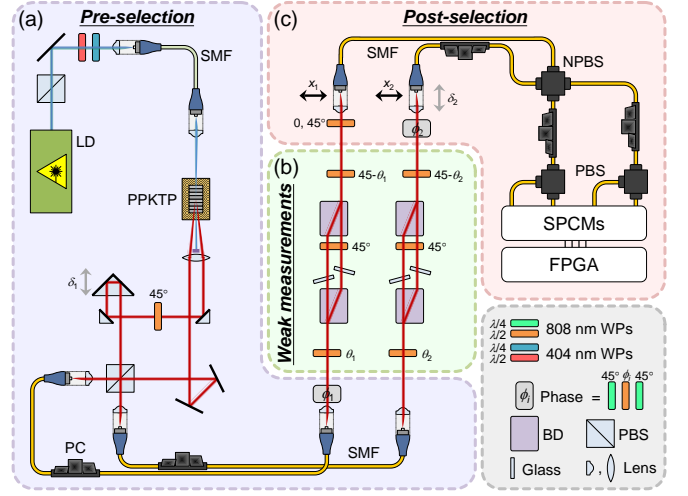


FIG. 2. Experimental setup. (a) Pre-selection. We use a non-collinear SPDC process with a PPKTP crystal and a compensation setup to generate a maximally polarization-entangled state. The polarization singlet state is prepared using PCs and ϕ_1 to adjust polarizations and phase in the SMFs. (b) Weak measurements. The spatial mode of each incidence beam is slightly separated into two parts. Their effective measurement bases are linearly polarized along $2\theta_i$ and $\frac{\pi}{2} + 2\theta_i$ from the horizontal axis so as to be orthogonal to each other. (c) Post-selection. The fiber-based Bell-state analyzer consists of an NPBS, two PBSs, and coincidence counters. Adding a HWP (0° or 45°), we can post-select two states ($|\psi^\pm\rangle$ or $|\phi^\pm\rangle$) among the four Bell states. LD: laser diode at 406 nm, PPKTP: periodically-poled KTiOPO_4 crystal; δ_i : optical delay line; PC: polarization controller; SMF: single-mode fiber; ϕ_i : phase controller consisting of WPs; NPBS: non-polarizing beam splitter; PBS: polarizing beam splitter; SPCM: single photon counting module; FPGA: coincidence counter; WP: wave-plate; BD: Calcite beam displacer.

idea is valid for all initial pure state, we perform experiment with the maximally entangled state since it exhibits the most dramatic result ([16], Sec. IV).

Figure 2 shows our experimental setup, which consists of three parts. *Pre-selection*: Using a spontaneous parametric down-conversion (SPDC) process for a periodically-poled KTiOPO_4 (PPKTP) crystal, we generate single-mode fiber (SMF) coupled polarization-entangled photon pairs [27]. Employing fiber polarization controllers (PC) and a polarization-dependent phase shifter ϕ_1 ([16], Sec. VII), we prepare the singlet state described as

$$|\psi^-\rangle = \frac{1}{\sqrt{2}} (|H\rangle|V\rangle - |V\rangle|H\rangle). \quad (4)$$

Here, $|H\rangle$ and $|V\rangle$ denote single-photon states linearly polarized in the horizontal and vertical directions, respectively. The spatial modes of the photons emitted from the SMFs are approximately Gaussian. *Weak measurements*: Each photon of a photon pair traverses a novel polarization weak-measurement apparatus [28]. Depend-

ing on the H and V polarizations, the spatial mode of the input beam is split and recombined by beam displacers (BD). According to Snell's law, two tilted glasses (2.5-mm thick) in both arms yield a polarization-dependent beam displacement at the output. The measurement strength or displacement can be adjusted by tilting the glass angles ([16], Sec. VIII), because the strength is defined as $s = g^2/(2\sigma^2)$ [25], where g is half the beam displacement and σ is the fixed width of the Gaussian intensity profile from the SMF ([16], Sec. IX). The weak-measurement bases equivalent to the displacement polarization bases (H , V) are effectively controlled by the half-wave plate (HWP) angle θ_i . *Post-selection*: The weakly measured (or disturbed) singlet state is post-selected to

two ($|\psi^\pm\rangle = |HV\rangle \pm |VH\rangle$ or $|\phi^\pm\rangle = |HH\rangle \pm |VV\rangle$) Bell states via a HWP (at 0° or 45°) and a Bell-state analyzer [29], consisting of fiber-optics beam splitters, compensators (PCs, ϕ_2 and δ_2) and a coincidence counter. The coincidence count (post-selection probability) distributions obtained by adjusting the fiber-coupler positions x_i are employed to calculate the measurement outcomes, i.e., the expectation values $\langle AB \rangle$ or $\langle AB \rangle_w$ ([16], Sec. II and III). We note that the SMF-based Bell-state analyzer and the detection probability distribution measurements are the essential components of this experiment, because the conventional probability distribution (pointer state) measurement method using a narrow slit [28, 30] is almost inapplicable to the Bell-state analyzer in free-space ([16], Sec. IX).

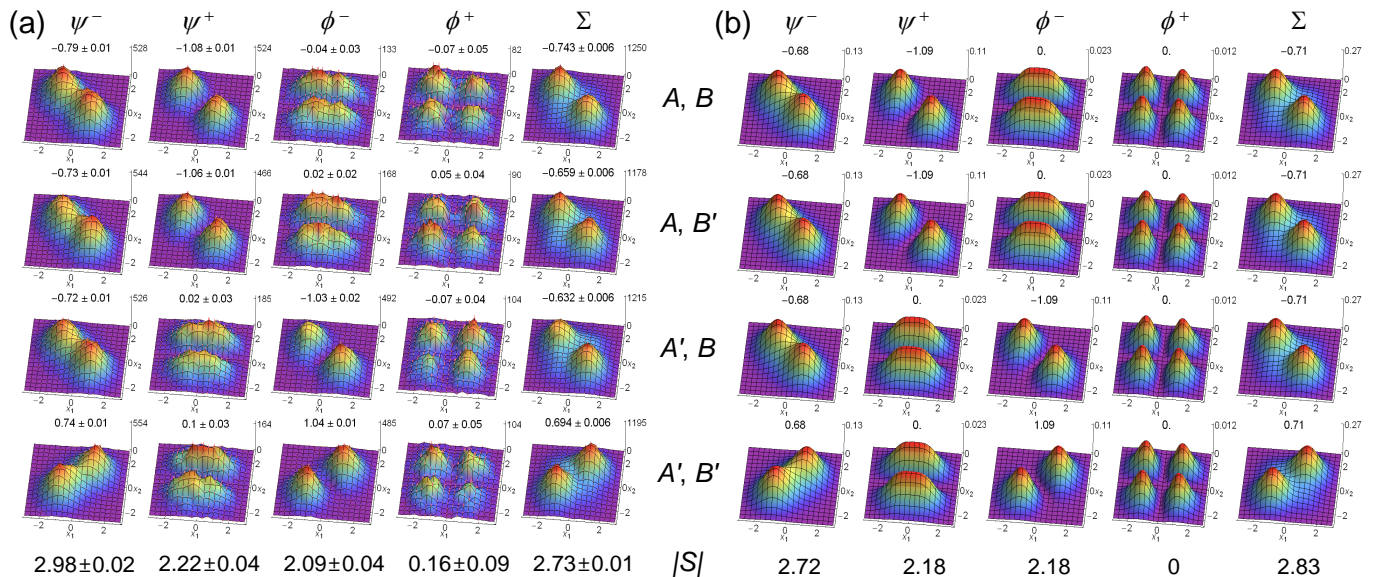


FIG. 3. Probability distributions, $\langle AB \rangle$, and $|S|$ for measurement strength $s \approx 1$. (a) Experimentally measured net coincidence count (per 1 s) distributions for four post-selected states (ψ^\pm , ϕ^\pm) and without post-selection (Σ). The Poissonian photon-counting errors are represented by pink error bars. The expectation values of the AB correlation are given on the top of each graph, with the standard error. The $|S|$ values obtained from summing these values for each column, which correspond to the $|S|$ values of the results post-selected to the state indicated at the top of the column, are presented at the bottom. (b) Detection probability distributions, identical to (a) but obtained theoretically.

The quantum mechanical counterparts of the classical polarization observables A and B , i.e., the Stokes parameters, are Pauli operators defined as $\vec{n} \cdot \vec{\sigma}$, where \vec{n} is a unit vector in Bloch space and $\vec{\sigma}$ is the Pauli vector [31]. Maximum violation of the CHSH inequality in equation (2) occurs when the observables are chosen to be $A = \hat{Z}$, $A' = \hat{X}$, $B = \frac{\hat{X} + \hat{Z}}{\sqrt{2}}$, and $B' = \frac{-\hat{X} + \hat{Z}}{\sqrt{2}}$. \hat{X} (\hat{Z}) is a Pauli operator along the x (z) axis in Bloch space. The corresponding measurement bases are provided by respective HWP angles of $\theta_1 = 0$, $\theta'_1 = \frac{\pi}{8}$, $\theta_2 = \frac{\pi}{16}$, and $\theta'_2 = -\frac{\pi}{16}$ [32]. With the bases for the maximum violation of the CHSH inequality, we obtained detection probability distributions depending on four post-selected Bell states, and calculated $\langle AB \rangle$ and $|S|$. Figure 3 shows

(a) experimentally measured coincidence counting distributions and (b) the corresponding theoretically calculated probability distributions ([16], Sec. X) with or without post-selection to the Bell states (ψ^\pm , ϕ^\pm), where the $\langle AB \rangle$ and $|S|$ calculated from the distributions are also shown at the top of each graph and at the bottom of each column, respectively. We normalize x_i with g_i , namely x_i/g_i . The error bar (in pink) associated with each data point in Fig. 3(a) represents the Poissonian photon-counting error. The experimental results are well-matched with the theoretical calculations shown in Fig. 3(b).

The most important result of our experiment is presented in Fig. 4. At post-selection, we acquire one among

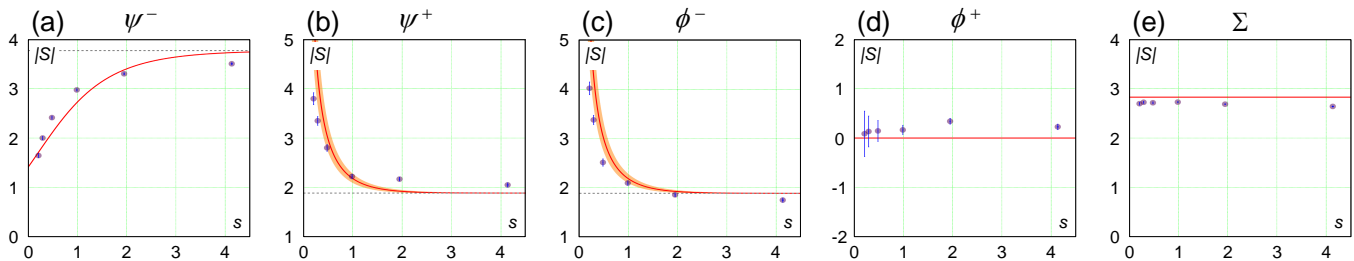


FIG. 4. Results of $|S|$. $|S|$ values post-selected to (a) ψ^- , (b) ψ^+ , (c) ϕ^- , and (d) ϕ^+ as functions of s , obtained both experimentally (points with error bars) and theoretically (red lines). (e) presents the $|S|$ obtained without post-selection. Note that, at the smallest s of 0.21, we believe DFM is effectively achieved, so that the $|S|$ of (a) becomes lower than the classical bound, while the $|S|$ of (e) always violates the CHSH inequality.

four Bell states ψ^- , ψ^+ , ϕ^- , and ϕ^+ , with respective probabilities of p_{ψ^-} , p_{ψ^+} , p_{ϕ^-} , and p_{ϕ^+} . Using the weak-measurement outcomes, we obtain the $|S|$ for each case as a function of s , denoted respectively as $|S_{\psi^-}|$, $|S_{\psi^+}|$, $|S_{\phi^-}|$, and $|S_{\phi^+}|$, which are presented in Fig. 4(a)–(d) and which range from 0.21 to 4.14. Fig. 4(a) demonstrates that $|S_{\psi^-}|$ decreases with decreasing s , becoming lower than 2, i.e., the classical bound of the CHSH inequality. This confirms our expectation that a quantum state exhibits classical behavior (by satisfying the CHSH inequality) when the measurement is performed with vanishing disturbance ($s \rightarrow 0$ and post-selection to the initial state). As shown in Fig. 4, the theoretical expectations (red curves) are reasonably well fit to our experimental results (dots).

Additionally, we experimentally obtained $p_{\psi^-} = 0.62$, $p_{\psi^+} = 0.18$, $p_{\phi^-} = 0.17$, and $p_{\phi^+} = 0.03$ for the smallest s value of 0.21. This chasm with the weak limit, $p_{\psi^-} \rightarrow 1$ and $p_i \rightarrow 0$ ($i = \psi^+, \phi^-, \phi^+$) at $s \rightarrow 0$, originates from the following realistic restrictions. First, it is difficult to obtain $s \rightarrow 0$ in experiment, because an infinite number of measurements are required in order to obtain meaningful information within this limit. Second, our post-selection suffers from errors. The reported Bell-state measurement success rate is as high as 95% [29]. However, our post-selection was performed after the weak measurements, which further decreases the success rate. Note that our success rate as regards the post-selection to the initial state (ψ^-) without the weak measurement and the scanning process is 93.3%.

We can negate the post-selection by summing over all possible outcome distributions, denoted as Σ in Fig. 3. From the total distribution, we calculated $\langle AB \rangle$ and $|S|$. The $|S_{\Sigma}|$ values without post-selection exhibit violation of the CHSH inequality as much as the initial state ψ^- should. In Fig. 4(e), $|S_{\Sigma}|$ lies well above the classical bound irrespective of s . This shows that the so-called “quantumness” of the initial Bell state, as indicated by the CHSH inequality violation, survives even after weak measurement is performed. It also explains why $|S_{\psi^+}|$

and $|S_{\phi^-}|$ diverge as s vanishes in Fig. 4(b) and (c) due to $|S_{\Sigma}| = 2\sqrt{2}$, $|S_{\psi^-}| = \sqrt{2}$, $p_{\psi^-} \rightarrow 1$, $p_{\psi^+} \rightarrow 0$, and $p_{\phi^-} \rightarrow 0$ within the limit $s \rightarrow 0$. We can ignore case (d), because $|S_{\phi^+}| = 0$ ([16], Sec. XI).

Finally, we discuss experimental errors. First, the strengths of the two weak measurements of A and B , assumed to be equal, differ within $\delta s = |s_A - s_B| \leq 0.15$, except when $s = 4.14$ ($\delta s \sim 0.33$). This introduces errors in the theoretical curves, indicated by the orange-shaded regions in Fig. 4(b) and (c), but negligibly small errors in Fig. 4(a), (d), and (e). Second, major experimental errors in the g_i , σ_i , $\langle AB \rangle$, and $|S|$ estimations is calculated (propagated) from Poissonian error of each photon counting raw data. They are represented as error bars in the figures showing the experimental result. In Fig. 4(b)–(d), the smaller the values of s , the larger these errors. This is because the post-selection success probability decreases with decreasing s for these results. Third, unquantified experimental errors exist, such as wavefront distortion and non-ideal parallelisms from the optics in weak measurement apparatus; thus, we surmise that those unexpected and additional state-disturbance errors yield non-ideal success probabilities for the Bell-state analyzer and slight differences between the experimental data and theoretical predictions.

In summary, we have shown both theoretically and experimentally that the outcomes of weak measurement of the initial Bell state consequently post-selected to the initial state exhibit classical behavior, in the sense that they satisfy the CHSH inequality. Without post-selection or summing over all possible post-selection outcomes, the results violate the CHSH inequality. This finding implies that, if one measures a quantum system without disturbance, the measurement outcomes behave classically. Measurement-induced disturbance is a core aspect of quantum mechanics.

This work was supported by the National Research Foundation of Korea (NRF) grants (No. 2014R1A1A2054719, 2015R1A2A1A05001819, 2016R1A2B4015978, 2016R1A4A1008978).

† moon.hanseb@gmail.com

‡ swkim0412@gmail.com

- [1] W. Heisenberg, *Zeitschrift für Physik* **43**, 172 (1927).
- [2] J. A. Wheeler and W. H. Zurek, eds., *Quantum Theory and Measurement*, 62–84 (Princeton University Press, 1983).
- [3] H. P. Robertson, *Phys. Rev.* **34**, 163 (1929).
- [4] M. Ozawa, *Phys. Rev. A* **67**, 042105 (2003).
- [5] P. Busch, P. Lahti, and R. F. Werner, *Phys. Rev. Lett.* **111**, 160405 (2013).
- [6] R. P. Feynman, R. B. Leighton, and M. Sands, *The Feynman Lectures on Physics*, Vol. 1 (Addison Wesley Longman, 1964) chapter 37.
- [7] S. Dürr, T. Nonn, and G. Rempe, *Nature* **395**, 33 (1998).
- [8] V. B. Braginsky, F. Y. Khalili, and K. S. Thorne, *Quantum Measurement* (Cambridge University Press, 1995).
- [9] C. A. Fuchs and A. Peres, *Phys. Rev. A* **53**, 2038 (1996).
- [10] K. Banaszek, *Phys. Rev. Lett.* **86**, 1366 (2001).
- [11] M. F. Sacchi, *Phys. Rev. Lett.* **96**, 220502 (2006).
- [12] L. Maccone, *Phys. Rev. A* **73**, 042307 (2006).
- [13] H. Terashima, *Phys. Rev. A* **83**, 032114 (2011).
- [14] H. Terashima, *Phys. Rev. A* **85**, 022124 (2012).
- [15] L. Fan, W. Ge, H. Nha, and M. S. Zubairy, *Phys. Rev. A* **92**, 022114 (2015).
- [16] See supplemental material for details.
- [17] Y. Aharonov, D. Z. Albert, and L. Vaidman, *Phys. Rev. Lett.* **60**, 1351 (1988).
- [18] W. H. Zurek, *Phys. Rev. D* **26**, 1862 (1982).
- [19] J. Kofler and C. Brukner, *Phys. Rev. Lett.* **99**, 180403 (2007).
- [20] H. Jeong, Y. Lim, and M. S. Kim, *Phys. Rev. Lett.* **112**, 010402 (2014).
- [21] G. C. Ghirardi, A. Rimini, and T. Weber, *Phys. Rev. D* **34**, 470 (1986).
- [22] J. F. Clauser, M. A. Horne, A. Shimony, and R. A. Holt, *Phys. Rev. Lett.* **23**, 880 (1969).
- [23] K. J. Resch and A. M. Steinberg, *Phys. Rev. Lett.* **92**, 130402 (2004).
- [24] S. Wu and Y. Li, *Phys. Rev. A* **83**, 052106 (2011).
- [25] K. Nakamura, A. Nishizawa, and M.-K. Fujimoto, *Phys. Rev. A* **85**, 012113 (2012).
- [26] A. J. Leggett and A. Garg, *Phys. Rev. Lett.* **54**, 857 (1985).
- [27] S. M. Lee, H. Kim, M. Cha, and H. S. Moon, *Opt. Express* **24**, 2941 (2016).
- [28] B. L. Higgins, M. S. Palsson, G. Y. Xiang, H. M. Wiseman, and G. J. Pryde, *Phys. Rev. A* **91**, 012113 (2015).
- [29] K. Mattle, H. Weinfurter, P. G. Kwiat, and A. Zeilinger, *Phys. Rev. Lett.* **76**, 4656 (1996).
- [30] N. W. M. Ritchie, J. G. Story, and R. G. Hulet, *Phys. Rev. Lett.* **66**, 1107 (1991).
- [31] M. Paris and J. Řeháček, eds., *Quantum State Estimation* (Springer, 2004) chapter 4.
- [32] P. G. Kwiat, K. Mattle, H. Weinfurter, A. Zeilinger, A. V. Sergienko, and Y. Shih, *Phys. Rev. Lett.* **75**, 4337 (1995).

Supplemental material for “Classicality from quantumness revealed by disturbance-free measurement”

Sang Min Lee^{1,2}, Minsu Kim¹, Heonoh Kim¹, Han Seb Moon¹, and Sang Wook Kim³

¹*Department of Physics, Pusan National University, Busan 46241, South Korea*

²*Korea Research Institute of Standards and Science, Daejeon 34113, South Korea and*

³*Department of Physics Education, Pusan National University, Busan 46241, South Korea*

I. MEASUREMENT-INDUCED DISTURBANCE

Here, we describe our weak-measurement procedure. For simplicity, we consider a two-state system and the measurement device described by observables \hat{A} and \hat{P} , respectively. The interaction between the two-state system and device is expressed as

$$\hat{H} = g\delta(t - t_0)\hat{A}\hat{P}, \quad (\text{I-1})$$

where g denotes the coupling constant and $\delta(\cdot)$ is a Dirac-delta function implying that the measurement is instantaneously performed at time t_0 . The device state described by the Gaussian probability distribution

$$|\psi_d(x)\rangle^2 = |\langle x|\psi_d\rangle|^2 = \frac{1}{n^2}e^{-\frac{x^2}{2\sigma^2}}, \quad (\text{I-2})$$

where $n = \sqrt{\sqrt{2\pi}\sigma}$ and σ is the Gaussian width, moves along the x axis depending on the \hat{A} value of the system, as \hat{P} is the momentum operator of the measurement device. x acts as the device pointer. If the system initially lies at $|\psi_s\rangle = \alpha|1\rangle_A + \beta|-1\rangle_A$, where $|1\rangle_A$ and $|-1\rangle_A$ denote the bases of \hat{A} , the total system after interaction with the device is expressed as

$$\langle x|\Psi\rangle = \alpha|1\rangle\frac{1}{n}e^{-\frac{(x-g)^2}{4\sigma^2}} + \beta|-1\rangle\frac{1}{n}e^{-\frac{(x+g)^2}{4\sigma^2}}. \quad (\text{I-3})$$

Tracing the device, we obtain the system density matrix

$$\rho'_s = \text{Tr}_d|\Psi\rangle\langle\Psi| = \begin{pmatrix} |\alpha|^2 & \alpha\beta^*\gamma \\ \alpha^*\beta\gamma & |\beta|^2 \end{pmatrix}, \quad (\text{I-4})$$

where γ represents the overlap between two device states moving to $+g$ and $-g$, that is,

$$\gamma = \int \frac{1}{n^2}e^{-\frac{(x-g)^2}{4\sigma^2}}e^{-\frac{(x+g)^2}{4\sigma^2}}dx = e^{-\frac{g^2}{2\sigma^2}} = e^{-s}. \quad (\text{I-5})$$

Here, the measurement strength s is introduced [1]. Below, we set $g = 1$, as s is determined from the ratio of g to σ . ρ'_s is decomposed into

$$\rho'_s = \frac{1+\gamma}{2}|\psi_s\rangle\langle\psi_s| + \frac{1-\gamma}{2}|\bar{\psi}_s\rangle\langle\bar{\psi}_s|, \quad (\text{I-6})$$

where $|\bar{\psi}_s\rangle = \alpha|1\rangle_A - \beta|-1\rangle_A$, a mirror symmetric state with $\langle\psi_s|\bar{\psi}_s\rangle = \cos\theta$, as shown in Fig. 1. Geometrically, ρ_s is located at a point along a straight line connecting $|\psi_s\rangle$ and $|\bar{\psi}_s\rangle$ in the Bloch sphere. The initial pure-state vector decreases in length in response to the measurement-induced decoherence. After weak measurement, there exists a probability that the state continues to survive at the initial state, which is expressed as $\frac{1+\gamma}{2}$. We then find the disturbance

$$D = 1 - \langle\psi_s|\rho'_s|\psi_s\rangle = \frac{1-\gamma}{2}\sin^2\theta \leq \frac{1-\gamma}{2}. \quad (\text{I-7})$$

At the weak-measurement limit, i.e., $s \ll 1$, we obtain $D < s$, implying that the disturbance is negligible.

The above argument is also applied to higher-dimensional states. After measurement, the state is decomposed into

$$|\psi_s\rangle\langle\psi_s| \xrightarrow{\text{measurement}} (1-p)|\psi_s\rangle\langle\psi_s| + p\sum_i c_i|\bar{\psi}_i\rangle\langle\bar{\psi}_i|, \quad (\text{I-8})$$

where $\sum_i c_i = 1$. p must be minimized, as such decomposition is not unique. We then obtain

$$D \leq \min\{p\}. \quad (\text{I-9})$$

In the weak-measurement limit, we intuitively recognize that $p \rightarrow 0$.

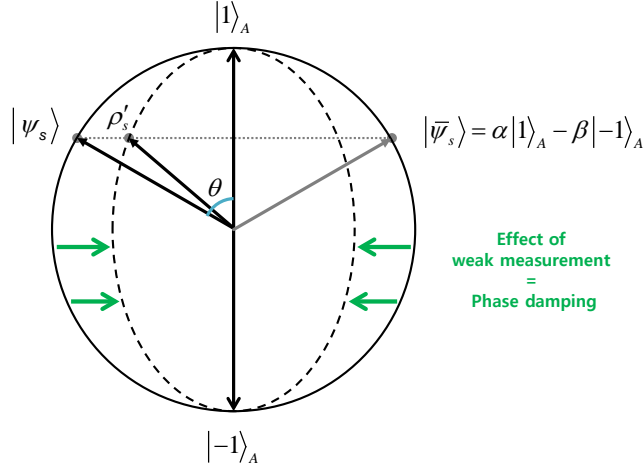


FIG. I.1. Depiction of system qubit state during measurement.

II. OPERATOR EXPECTATION VALUES

Here, we show that the average of the weak-measurement outcomes described in Sec. I are equivalent to the quantum mechanical average. After the interaction between the system and device, the total system is described as given in equation (I-3). Tracing the system, we obtain the device-pointer probability distribution

$$p(x) = \frac{1}{n^2} \left(|\alpha|^2 e^{-\frac{(x-1)^2}{2\sigma^2}} + |\beta|^2 e^{-\frac{(x+1)^2}{2\sigma^2}} \right). \quad (\text{II-1})$$

The average of the pointer positions is equal to the expectation value of the \hat{A} operator, such that

$$\langle x \rangle = \int x p(x) dx = |\alpha|^2 - |\beta|^2 = \langle \hat{A} \rangle. \quad (\text{II-2})$$

We emphasize that this does not depend on the measurement uncertainty σ (or s), because the center of the pointer probability distribution remains intact regardless of the magnitude of σ . In conventional experiments, this is acceptable, because the center values of moved distributions correspond to the eigen-values. We will show that this is also true in our experiment. This argument has also been applied to more generalized cases, such as for multi-dimensional and multi-partite systems and for weak values incorporating post-selection [1].

III. JOINT WEAK VALUE

Here, we show the calculation method for the joint weak value of two observables \hat{A} and \hat{B} . Our strategy is as follows. First, we find the device density matrix ρ'_d , measuring \hat{A} and \hat{B} . The corresponding pointers of these observables are \hat{X}_1 and \hat{X}_2 , respectively, when both weak measurement and post-selection are completed. Then, we calculate the average of \hat{X}_1 and \hat{X}_2 , i.e., $\text{Tr}(\hat{X}_1 \hat{X}_2 \rho'_d)$.

The interaction Hamiltonian is expressed as

$$\hat{H} = g_1 \delta(t - t_o) \hat{A} \hat{P}_1 + g_2 \delta(t - t_o) \hat{B} \hat{P}_2, \quad (\text{III-1})$$

where g_1 and g_2 denote coupling constants, \hat{P}_1 and \hat{P}_2 are the momentum operators related to the pointer-state position operators \hat{X}_1 and \hat{X}_2 , and t_o is the time until the measurement. We assume that $g_1 = g_2 = g$ for simplicity, and that \hat{A} and \hat{B} satisfy $\hat{A}^2 = \hat{B}^2 = I$, where I is the identity. The initial system state is an arbitrary two-qubit state denoted as $|\psi_i\rangle$, and the measurement device is prepared as a wavefunction of the normalized two-dimensional Gaussian distribution

$$\langle x_1, x_2 | \Phi \rangle = \Phi(x_1, x_2) = \frac{1}{\sqrt{2\pi\sigma_1\sigma_2}} \exp\left(-\frac{x_1^2}{4\sigma_1^2}\right) \exp\left(-\frac{x_2^2}{4\sigma_2^2}\right), \quad (\text{III-2})$$

where σ_1 and σ_2 are the probability distribution widths in x_1 and x_2 , respectively. After the interaction between the system and the measurement device, which is described by the unitary evolution $U = e^{-ig(\hat{A}\hat{P}_1 + \hat{B}\hat{P}_2)}$, the total system state is expressed as

$$\begin{aligned} \rho' &\equiv U\rho U^\dagger, \\ &= \rho + \sum_{n=1}^{\infty} \frac{(-ig)^n}{n!} \mathbf{ad}^n[\hat{A}\hat{P}_1 \circ \rho] + \sum_{m=1}^{\infty} \frac{(-ig)^m}{m!} \mathbf{ad}^m[\hat{B}\hat{P}_2 \circ \rho] + \sum_{n,m=1}^{\infty} \frac{(-ig)^n}{n!} \frac{(-ig)^m}{m!} \mathbf{ad}^n[\hat{A}\hat{P}_1 \circ (\mathbf{ad}^m[\hat{B}\hat{P}_2 \circ \rho])], \end{aligned} \quad (\text{III-3})$$

where ρ is the initial total density matrix, $\mathbf{ad}^1[\Omega \circ \Theta] \equiv [\Omega, \Theta]$, and $\mathbf{ad}^n[\Omega \circ \Theta] \equiv \mathbf{ad}[\Omega \circ (\mathbf{ad}^{n-1}[\Omega \circ \Theta])] = [\Omega, \mathbf{ad}^{n-1}[\Omega \circ \Theta]]$. Tracing the measurement device, we obtain the system density matrix

$$\begin{aligned} \rho'_s &= \text{Tr}_d \rho', \\ &= \rho_s + \sum_{n=1}^{\infty} \frac{(-ig)^n \langle \hat{P}_1^n \rangle}{n!} \mathbf{ad}^n[\hat{A} \circ \rho_s] + \sum_{m=1}^{\infty} \frac{(-ig)^m \langle \hat{P}_2^m \rangle}{m!} \mathbf{ad}^m[\hat{B} \circ \rho_s] \\ &\quad + \sum_{n,m=1}^{\infty} \frac{(-ig)^n \langle \hat{P}_1^n \rangle}{n!} \frac{(-ig)^m \langle \hat{P}_2^m \rangle}{m!} \mathbf{ad}^n[\hat{A} \circ (\mathbf{ad}^m[\hat{B} \circ \rho_s])], \end{aligned} \quad (\text{III-4})$$

where $\langle \hat{P}^n \rangle \equiv \text{Tr}_d(\hat{P}^n \rho_d)$.

Tracing the system, the measurement-device density matrix after post-selection on the state $|\psi_f\rangle$ is expressed as

$$\rho'_d = \frac{\text{Tr}_s \rho' \Pi_f}{\text{Tr} \rho' \Pi_f}, \quad (\text{III-5})$$

where $\Pi_f = |\psi_f\rangle\langle\psi_f|$. To calculate equation (III-5) in the form of the weak value, we rewrite this expression as

$$\rho'_d = \frac{Z \rho'_d}{Z}, \quad (\text{III-6})$$

where $Z = \text{Tr} \rho' \Pi_f / |\langle\psi_f|\psi_i\rangle|^2$ and $Z \rho'_d = \text{Tr}_s \rho' \Pi_f / |\langle\psi_f|\psi_i\rangle|^2$, if $\langle\psi_f|\psi_i\rangle \neq 0$. Below, we calculate Z and $Z \rho'_d$ separately. The case of $\langle\psi_f|\psi_i\rangle = 0$ is considered in subsection III B.

A. Non-orthogonal weak value

From equation (III-3), we obtain

$$\begin{aligned} Z &= 1 + \sum_{n=1}^{\infty} \frac{(-ig)^n \langle \hat{P}_1^n \rangle}{n!} \sum_{j=0}^n (-1)^j {}_n C_j \langle \hat{A}^{n-j} \rangle_w \langle \hat{A}^j \rangle_w^* + \sum_{m=1}^{\infty} \frac{(-ig)^m \langle \hat{P}_2^m \rangle}{m!} \sum_{k=0}^m (-1)^k {}_m C_k \langle \hat{B}^{m-k} \rangle_w \langle \hat{B}^k \rangle_w^* \\ &\quad + \sum_{n,m=1}^{\infty} \frac{(-ig)^n \langle \hat{P}_1^n \rangle}{n!} \frac{(-ig)^m \langle \hat{P}_2^m \rangle}{m!} \sum_{j=0}^n (-1)^j {}_n C_j \sum_{k=0}^m (-1)^k {}_m C_k \langle \hat{A}^{n-j} \hat{B}^{m-k} \rangle_w \langle \hat{A}^j \hat{B}^k \rangle_w^*, \end{aligned} \quad (\text{III-7})$$

$$= Z_1 + Z_2, \quad (\text{III-8})$$

where $s_i \equiv g^2 / (2\sigma_i^2) = 2g^2 \langle \hat{P}_i^2 \rangle$ is the strength of the weak measurement, $\langle O \rangle_w = \langle\psi_f|O|\psi_i\rangle / \langle\psi_f|\psi_i\rangle$,

$$Z_1 = 1 + \frac{1}{2}(1 - |\langle \hat{A} \rangle_w|^2)(e^{-s_1} - 1) + \frac{1}{2}(1 - |\langle \hat{B} \rangle_w|^2)(e^{-s_2} - 1), \quad (\text{III-9})$$

and

$$\begin{aligned}
Z_2 = & \left[\left(\sum_{n=1}^{\infty} \frac{(-ig)^{2n} \langle \hat{P}_1^{2n} \rangle}{(2n)!} \sum_{j=0}^{2n} (-1)^j {}_{2n}C_j \right) \left(\sum_{m=1}^{\infty} \frac{(-ig)^{2m} \langle \hat{P}_2^{2m} \rangle}{(2m)!} \sum_{k=0}^{2m} (-1)^k {}_{2m}C_k \right) \langle \hat{A}^{2n-j} \hat{B}^{2m-k} \rangle_w \langle \hat{A}^j \hat{B}^k \rangle_w^* \right. \\
& + \left(\sum_{n=1}^{\infty} \frac{(-ig)^{2n} \langle \hat{P}_1^{2n} \rangle}{(2n)!} \sum_{j=0}^{2n} (-1)^j {}_{2n}C_j \right) \left(\sum_{m=0}^{\infty} \frac{(-ig)^{2m+1} \langle \hat{P}_2^{2m+1} \rangle}{(2m+1)!} \sum_{k=0}^{2m+1} (-1)^k {}_{2m+1}C_k \right) \langle \hat{A}^{2n-j} \hat{B}^{2m+1-k} \rangle_w \langle \hat{A}^j \hat{B}^k \rangle_w^* \\
& + \left(\sum_{n=0}^{\infty} \frac{(-ig)^{2n+1} \langle \hat{P}_1^{2n+1} \rangle}{(2n+1)!} \sum_{j=0}^{2n+1} (-1)^j {}_{2n+1}C_j \right) \left(\sum_{m=1}^{\infty} \frac{(-ig)^{2m} \langle \hat{P}_2^{2m} \rangle}{(2m)!} \sum_{k=0}^{2m} (-1)^k {}_{2m}C_k \right) \langle \hat{A}^{2n+1-j} \hat{B}^{2m-k} \rangle_w \langle \hat{A}^j \hat{B}^k \rangle_w^* \\
& + \left. \left(\sum_{n=0}^{\infty} \frac{(-ig)^{2n+1} \langle \hat{P}_1^{2n+1} \rangle}{(2n+1)!} \sum_{j=0}^{2n+1} (-1)^j {}_{2n+1}C_j \right) \left(\sum_{m=0}^{\infty} \frac{(-ig)^{2m+1} \langle \hat{P}_2^{2m+1} \rangle}{(2m+1)!} \sum_{k=0}^{2m+1} (-1)^k {}_{2m+1}C_k \right) \right. \\
& \quad \left. \times \langle \hat{A}^{2n+1-j} \hat{B}^{2m+1-k} \rangle_w \langle \hat{A}^j \hat{B}^k \rangle_w^* \right]. \tag{III-10}
\end{aligned}$$

Using $\langle \hat{P}_i^{2n+1} \rangle = 0$, $\langle \hat{P}_i^{2n} \rangle = (2n-1)!! \langle \hat{P}_i^2 \rangle^n$ and $\sum_{j=0}^n {}_{2n}C_{2j} = \sum_{j=0}^{n-1} {}_{2n}C_{2j+1} = 2^{2n-1}$, Z_2 is rewritten as

$$\begin{aligned}
Z_2 = & \sum_{n=1}^{\infty} \frac{(-ig)^{2n} (2n-1)!! \langle \hat{P}_1^2 \rangle^n}{(2n)!} \sum_{j=0}^{2n} (-1)^j {}_{2n}C_j \sum_{m=1}^{\infty} \frac{(-ig)^{2m} (2m-1)!! \langle \hat{P}_2^2 \rangle^m}{(2m)!} \sum_{k=0}^{2m} (-1)^k {}_{2m}C_k \langle \hat{A}^{2n-j} \hat{B}^{2m-k} \rangle_w \langle \hat{A}^j \hat{B}^k \rangle_w^*, \\
= & \sum_{n=1}^{\infty} \frac{(-1)^n (g)^{2n} \langle \hat{P}_1^2 \rangle^n}{2^n n!} \sum_{m=1}^{\infty} \frac{(-1)^m (g)^{2m} \langle \hat{P}_2^2 \rangle^m}{2^m m!} (2^{2n+2m-2}) (1 - |\langle \hat{A} \rangle_w|^2 - |\langle \hat{B} \rangle_w|^2 + |\langle \hat{A} \hat{B} \rangle_w|^2), \\
= & \frac{1}{4} (1 - |\langle \hat{A} \rangle_w|^2 - |\langle \hat{B} \rangle_w|^2 + |\langle \hat{A} \hat{B} \rangle_w|^2) (e^{-s_1} - 1) (e^{-s_2} - 1). \tag{III-11}
\end{aligned}$$

We finally obtain

$$\begin{aligned}
Z = & 1 + \frac{1}{2} (1 - |\langle \hat{A} \rangle_w|^2) (e^{-s_1} - 1) + \frac{1}{2} (1 - |\langle \hat{B} \rangle_w|^2) (e^{-s_2} - 1) \\
& + \frac{1}{4} (1 - |\langle \hat{A} \rangle_w|^2 - |\langle \hat{B} \rangle_w|^2 + |\langle \hat{A} \hat{B} \rangle_w|^2) (e^{-s_1} - 1) (e^{-s_2} - 1). \tag{III-12}
\end{aligned}$$

Note that $Z \rightarrow 1$ as $s_{1,2} \rightarrow 0$.

Now, we calculate $Z\rho'_d$. From equations (III-3), (III-5), and (III-6), we obtain

$$\begin{aligned}
Z\rho'_d = & \left[\rho_d^1 \rho_d^2 + \sum_{n,m=1}^{\infty} \frac{(-ig)^{2n}(-ig)^{2m}}{(2n)!(2m)!} \left(\sum_{j=0}^n {}_{2n}C_{2j} \hat{P}_1^{2n-2j} \rho_d^1 \hat{P}_1^{2j} \sum_{k=0}^m {}_{2m}C_{2k} \hat{P}_2^{2m-2k} \rho_d^2 \hat{P}_2^{2k} \right. \right. \\
& - |\langle \hat{A} \rangle_w|^2 \sum_{j=0}^n {}_{2n}C_{2j} \hat{P}_1^{2n-2j} \rho_d^1 \hat{P}_1^{2j} \sum_{k=0}^{m-1} {}_{2m}C_{2k+1} \hat{P}_2^{2m-2k-1} \rho_d^2 \hat{P}_2^{2k+1} \\
& - |\langle \hat{B} \rangle_w|^2 \sum_{j=0}^{n-1} {}_{2n}C_{2j+1} \hat{P}_1^{2n-2j-1} \rho_d^1 \hat{P}_1^{2j+1} \sum_{k=0}^m {}_{2m}C_{2k} \hat{P}_2^{2m-2k} \rho_d^2 \hat{P}_2^{2k} \\
& + |\langle \hat{A}\hat{B} \rangle_w|^2 \sum_{j=0}^{n-1} {}_{2n}C_{2j+1} \hat{P}_1^{2n-2j-1} \rho_d^1 \hat{P}_1^{2j+1} \sum_{k=0}^{m-1} {}_{2m}C_{2k+1} \hat{P}_2^{2m-2k-1} \rho_d^2 \hat{P}_2^{2k+1} \left. \right) \\
& + \sum_{n=1}^{\infty} \frac{(-ig)^{2n}}{(2n)!} \sum_{m=0}^{\infty} \frac{(-ig)^{2m+1}}{(2m+1)!} \left(\langle \hat{B} \rangle_w \sum_{j=0}^n {}_{2n}C_{2j} \hat{P}_1^{2n-2j} \rho_d^1 \hat{P}_1^{2j} \sum_{k=0}^m {}_{2m+1}C_{2k} \hat{P}_2^{2m+1-2k} \rho_d^2 \hat{P}_2^{2k} \right. \\
& - \langle \hat{B} \rangle_w^* \sum_{j=0}^n {}_{2n}C_{2j} \hat{P}_1^{2n-2j} \rho_d^1 \hat{P}_1^{2j} \sum_{k=0}^{m-1} {}_{2m+1}C_{2k+1} \hat{P}_2^{2m-2k} \rho_d^2 \hat{P}_2^{2k+1} \\
& - \langle \hat{A}\hat{B} \rangle_w \langle \hat{A} \rangle_w^* \sum_{j=0}^{n-1} {}_{2n}C_{2j+1} \hat{P}_1^{2n-2j-1} \rho_d^1 \hat{P}_1^{2j+1} \sum_{k=0}^m {}_{2m+1}C_{2k} \hat{P}_2^{2m+1-2k} \rho_d^2 \hat{P}_2^{2k} \\
& + \langle \hat{A} \rangle_w \langle \hat{A}\hat{B} \rangle_w^* \sum_{j=0}^{n-1} {}_{2n}C_{2j+1} \hat{P}_1^{2n-2j-1} \rho_d^1 \hat{P}_1^{2j+1} \sum_{k=0}^{m-1} {}_{2m+1}C_{2k+1} \hat{P}_2^{2m-2k} \rho_d^2 \hat{P}_2^{2k+1} \left. \right) \\
& + \sum_{n=0}^{\infty} \frac{(-ig)^{2n+1}}{(2n+1)!} \sum_{m=1}^{\infty} \frac{(-ig)^{2m}}{(2m)!} \left(\langle \hat{A} \rangle_w \sum_{j=0}^n {}_{2n+1}C_{2j} \hat{P}_1^{2n+1-2j} \rho_d^1 \hat{P}_1^{2j} \sum_{k=0}^m {}_{2m}C_{2k} \hat{P}_2^{2m-2k} \rho_d^2 \hat{P}_2^{2k} \right. \\
& - \langle \hat{A}\hat{B} \rangle_w \langle \hat{B} \rangle_w^* \sum_{j=0}^n {}_{2n+1}C_{2j} \hat{P}_1^{2n+1-2j} \rho_d^1 \hat{P}_1^{2j} \sum_{k=0}^{m-1} {}_{2m}C_{2k+1} \hat{P}_2^{2m-2k-1} \rho_d^2 \hat{P}_2^{2k+1} \\
& - \langle \hat{A} \rangle_w^* \sum_{j=0}^{n-1} {}_{2n+1}C_{2j+1} \hat{P}_1^{2n-2j} \rho_d^1 \hat{P}_1^{2j+1} \sum_{k=0}^m {}_{2m}C_{2k} \hat{P}_2^{2m-2k} \rho_d^2 \hat{P}_2^{2k} \\
& + \langle \hat{B} \rangle_w \langle \hat{A}\hat{B} \rangle_w^* \sum_{j=0}^{n-1} {}_{2n+1}C_{2j+1} \hat{P}_1^{2n-2j} \rho_d^1 \hat{P}_1^{2j+1} \sum_{k=0}^{m-1} {}_{2m}C_{2k+1} \hat{P}_2^{2m-2k-1} \rho_d^2 \hat{P}_2^{2k+1} \left. \right) \\
& + \sum_{n=0}^{\infty} \frac{(-ig)^{2n+1}}{(2n+1)!} \sum_{m=0}^{\infty} \frac{(-ig)^{2m+1}}{(2m+1)!} \left(\langle \hat{A}\hat{B} \rangle_w \sum_{j=0}^n {}_{2n+1}C_{2j} \hat{P}_1^{2n+1-2j} \rho_d^1 \hat{P}_1^{2j} \sum_{k=0}^m {}_{2m+1}C_{2k} \hat{P}_2^{2m+1-2k} \rho_d^2 \hat{P}_2^{2k} \right. \\
& - \langle \hat{A} \rangle_w \langle \hat{B} \rangle_w^* \sum_{j=0}^n {}_{2n+1}C_{2j} \hat{P}_1^{2n+1-2j} \rho_d^1 \hat{P}_1^{2j} \sum_{k=0}^{m-1} {}_{2m+1}C_{2k+1} \hat{P}_2^{2m-2k} \rho_d^2 \hat{P}_2^{2k+1} \\
& - \langle \hat{B} \rangle_w \langle \hat{A} \rangle_w^* \sum_{j=0}^{n-1} {}_{2n+1}C_{2j+1} \hat{P}_1^{2n-2j} \rho_d^1 \hat{P}_1^{2j+1} \sum_{k=0}^m {}_{2m+1}C_{2k} \hat{P}_2^{2m+1-2k} \rho_d^2 \hat{P}_2^{2k} \\
& + \langle \hat{A}\hat{B} \rangle_w^* \sum_{j=0}^{n-1} {}_{2n+1}C_{2j+1} \hat{P}_1^{2n-2j} \rho_d^1 \hat{P}_1^{2j+1} \sum_{k=0}^{m-1} {}_{2m+1}C_{2k+1} \hat{P}_2^{2m-2k} \rho_d^2 \hat{P}_2^{2k+1} \left. \right) \Big]. \tag{III-13}
\end{aligned}$$

The pointer-position expectation values in the weak-value scheme discussed above are expressed as

$$\langle \psi_f | \hat{X}_j | \psi_i \rangle' \equiv Tr(\hat{X}_j \rho'_d), \quad \langle \psi_f | \hat{X}_1 \hat{X}_2 | \psi_i \rangle' \equiv Tr(\hat{X}_1 \hat{X}_2 \rho'_d). \tag{III-14}$$

We emphasize here that $\langle \cdot \rangle'$ is not a simple quantum mechanical average but, rather, a weak value of $|\psi_i\rangle$ post-selected as $|\psi_f\rangle$. Using equations (III-19), (III-14), $\langle \hat{X} \hat{P}^n + \hat{P}^n \hat{X} \rangle = 0$ (for $n \geq 1$), and $[\hat{X}, \hat{P}] = i$, we find

$$\langle \psi_f | \hat{X}_i \hat{X}_j | \psi_i \rangle' = \frac{1}{2Z} (\text{Re}[\langle \hat{A}\hat{B} \rangle_w + \langle \hat{A} \rangle_w \langle \hat{B} \rangle_w^*]), \tag{III-15}$$

where we set $g = 1$ without loss of generality.

To achieve measurement without disturbing the system, we simply set the final post-selected state to the initial state, as the undisturbed state should correspond to the original state. Thus, the outcome of the disturbance-free measurement (DFM) of two observables is expressed as

$$\langle \hat{X}_1 \hat{X}_2 \rangle_{\text{DFM}} = \langle \psi_i | \hat{X}_1 \hat{X}_2 | \psi_i \rangle' = \frac{1}{2} \left(\langle \hat{A} \hat{B} \rangle + \langle \hat{A} \rangle \langle \hat{B} \rangle \right). \quad (\text{III-16})$$

Note that, in equation (III-16), the weak value $\langle \cdot \rangle_w$ is replaced by the average $\langle \cdot \rangle$.

B. Orthogonal weak value

If $\langle \psi_f | \psi_i \rangle = 0$, we must calculate Z and $Z\rho'_d$ in a slightly different way. The denominator of equation (III-5) is calculated as

$$\begin{aligned} \text{Tr} \rho' \Pi_f &= \sum_{n=1}^{\infty} \frac{(-ig)^n \langle \hat{P}_1^n \rangle}{n!} \sum_{j=0}^n (-1)^j {}_n C_j \langle \psi_f | \hat{A}^{n-j} | \psi_i \rangle \langle \psi_i | \hat{A}^j | \psi_f \rangle \\ &+ \sum_{m=1}^{\infty} \frac{(-ig)^m \langle \hat{P}_2^m \rangle}{m!} \sum_{k=0}^m (-1)^k {}_m C_k \langle \psi_f | \hat{B}^{m-k} | \psi_i \rangle \langle \psi_i | \hat{B}^k | \psi_f \rangle \\ &+ \sum_{n,m=1}^{\infty} \frac{(-ig)^n \langle \hat{P}_1^n \rangle}{n!} \frac{(-ig)^m \langle \hat{P}_2^m \rangle}{m!} \sum_{j=0}^n (-1)^j {}_n C_j \sum_{k=0}^m (-1)^k {}_m C_k \langle \psi_f | \hat{A}^{n-j} \hat{B}^{m-k} | \psi_i \rangle \langle \psi_i | \hat{A}^j \hat{B}^k | \psi_f \rangle, \\ &= g^2 \langle \hat{P}_1^2 \rangle |\langle \psi_f | \hat{A} | \psi_i \rangle|^2 \left[1 + \sum_{n=1}^{\infty} \frac{(-ig)^n \langle \hat{P}_1^{n+2} \rangle}{n! \langle \hat{P}_1^2 \rangle} \sum_{j=0}^n (-1)^j {}_n C_j \langle \hat{A}^{n-j} \rangle_{ow} \langle \hat{A}^j \rangle_{ow}^* \right] \\ &+ g^2 \langle \hat{P}_2^2 \rangle |\langle \psi_f | \hat{B} | \psi_i \rangle|^2 \left[1 + \sum_{m=1}^{\infty} \frac{(-ig)^m \langle \hat{P}_2^{m+2} \rangle}{m! \langle \hat{P}_2^2 \rangle} \sum_{k=0}^m (-1)^k {}_m C_k \langle \hat{B}^{m-k} \rangle_{ow} \langle \hat{B}^k \rangle_{ow}^* \right] \\ &+ \sum_{n=1}^{\infty} \frac{(-ig)^{2n} \langle \hat{P}_1^{2n} \rangle}{(2n)!} \sum_{j=0}^{2n} (-1)^j {}_{2n} C_j \sum_{m=1}^{\infty} \frac{(-ig)^{2m} \langle \hat{P}_2^{2m} \rangle}{(2m)!} \sum_{k=0}^{2m} (-1)^k {}_{2m} C_k \langle \psi_f | \hat{A}^{2n-j} \hat{B}^{2m-k} | \psi_i \rangle \langle \psi_i | \hat{A}^j \hat{B}^k | \psi_f \rangle, \end{aligned} \quad (\text{III-17})$$

where $\langle \hat{A}^n \rangle_{ow} \equiv \langle \psi_f | \hat{A}^{n+1} | \psi_i \rangle / \langle \psi_f | \hat{A}^{n+1} | \psi_i \rangle$. Using $\langle \hat{P}_i^{2n+1} \rangle = 0$ and $\langle \hat{P}_i^{2n+2} \rangle = (2n+1)!! \langle \hat{P}_i^2 \rangle^{n+1}$ from equation (III-17), we obtain

$$\begin{aligned} \text{Tr} \rho' \Pi_f &= \frac{s_1}{2} \left(1 + \sum_{n=1}^{\infty} \frac{(-ig)^{2n} \langle \hat{P}_1^{2n} \rangle}{(2n+2)!!} \sum_{j=0}^{2n} \frac{(2n+2)!}{(2n-2j+1)!(2j+1)!} |\langle \psi_f | \hat{A} | \psi_i \rangle|^2 \right) \\ &+ \frac{s_2}{2} \left(1 + \sum_{m=1}^{\infty} \frac{(-ig)^{2m} \langle \hat{P}_2^{2m} \rangle}{(2m+2)!!} \sum_{k=0}^{2m} \frac{(2m+2)!}{(2m-2k+1)!(2k+1)!} |\langle \psi_f | \hat{B} | \psi_i \rangle|^2 \right) \\ &+ \sum_{n,m=1}^{\infty} \frac{(-ig)^{2n} (2n-1)!! \langle \hat{P}_1^{2n} \rangle}{(2n)!} \frac{(-ig)^{2m} (2m-1)!! \langle \hat{P}_2^{2m} \rangle}{(2m)!} \left(- \sum_{j=0}^{n-1} {}_{2n} C_{2j+1} \sum_{k=0}^m {}_{2m} C_{2k} |\langle \psi_f | \hat{A} | \psi_i \rangle|^2 \right. \\ &\quad \left. - \sum_{j=0}^n {}_{2n} C_{2j} \sum_{k=0}^{m-1} {}_{2m} C_{2k+1} |\langle \psi_f | \hat{B} | \psi_i \rangle|^2 + \sum_{j=0}^{n-1} {}_{2n} C_{2j+1} \sum_{k=0}^{m-1} {}_{2m} C_{2k+1} |\langle \psi_f | \hat{A} \hat{B} | \psi_i \rangle|^2 \right), \\ &= \frac{1}{2} |\langle \psi_f | \hat{A} | \psi_i \rangle|^2 (1 - e^{-s_1}) + \frac{1}{2} |\langle \psi_f | \hat{B} | \psi_i \rangle|^2 (1 - e^{-s_2}) \\ &+ \frac{1}{4} (|\langle \psi_f | \hat{A} \hat{B} | \psi_i \rangle|^2 - |\langle \psi_f | \hat{A} | \psi_i \rangle|^2 - |\langle \psi_f | \hat{B} | \psi_i \rangle|^2) (1 - e^{-s_1}) (1 - e^{-s_2}) \end{aligned} \quad (\text{III-18})$$

The numerator of equation (III-5) is calculated to be

$$\begin{aligned}
Tr_s \rho' \Pi_f = & \left[- \langle \psi_f | \hat{A} | \psi_i \rangle \langle \psi_i | \hat{A} | \psi_f \rangle \sum_{j=0}^n 2n C_{2j} \hat{P}_1^{2n-2j} \rho_d^1 \hat{P}_1^{2j} \sum_{k=0}^{m-1} 2m C_{2k+1} \hat{P}_2^{2m-2k-1} \rho_d^2 \hat{P}_2^{2k+1} \right. \\
& - \langle \psi_f | \hat{B} | \psi_i \rangle \langle \psi_i | \hat{B} | \psi_f \rangle \sum_{j=0}^{n-1} 2n C_{2j+1} \hat{P}_1^{2n-2j-1} \rho_d^1 \hat{P}_1^{2j+1} \sum_{k=0}^m 2m C_{2k} \hat{P}_2^{2m-2k} \rho_d^2 \hat{P}_2^{2k} \\
& + \langle \psi_f | \hat{A} \hat{B} | \psi_i \rangle \langle \psi_i | \hat{A} \hat{B} | \psi_f \rangle \sum_{j=0}^{n-1} 2n C_{2j+1} \hat{P}_1^{2n-2j-1} \rho_d^1 \hat{P}_1^{2j+1} \sum_{k=0}^{m-1} 2m C_{2k+1} \hat{P}_2^{2m-2k-1} \rho_d^2 \hat{P}_2^{2k+1} \\
& + \sum_{n=1}^{\infty} \frac{(-ig)^{2n}}{(2n)!} \sum_{m=0}^{\infty} \frac{(-ig)^{2m+1}}{(2m+1)!} \left(- \langle \psi_f | \hat{A} \hat{B} | \psi_i \rangle \langle \psi_i | \hat{A} | \psi_f \rangle \sum_{j=0}^{n-1} 2n C_{2j+1} \hat{P}_1^{2n-2j-1} \rho_d^1 \hat{P}_1^{2j+1} \sum_{k=0}^m 2m+1 C_{2k} \hat{P}_2^{2m+1-2k} \rho_d^2 \hat{P}_2^{2k} \right. \\
& + \langle \psi_f | \hat{A} | \psi_i \rangle \langle \psi_i | \hat{A} \hat{B} | \psi_f \rangle \sum_{j=0}^{n-1} 2n C_{2j+1} \hat{P}_1^{2n-2j-1} \rho_d^1 \hat{P}_1^{2j+1} \sum_{k=0}^{m-1} 2m+1 C_{2k+1} \hat{P}_2^{2m-2k} \rho_d^2 \hat{P}_2^{2k+1} \\
& + \sum_{n=0}^{\infty} \frac{(-ig)^{2n+1}}{(2n+1)!} \sum_{m=1}^{\infty} \frac{(-ig)^{2m}}{(2m)!} \left(- \langle \psi_f | \hat{A} \hat{B} | \psi_i \rangle \langle \psi_i | \hat{B} | \psi_f \rangle \sum_{j=0}^n 2n+1 C_{2j} \hat{P}_1^{2n+1-2j} \rho_d^1 \hat{P}_1^{2j} \sum_{k=0}^{m-1} 2m C_{2k+1} \hat{P}_2^{2m-2k-1} \rho_d^2 \hat{P}_2^{2k+1} \right. \\
& + \langle \psi_f | \hat{B} | \psi_i \rangle \langle \psi_i | \hat{A} \hat{B} | \psi_f \rangle \sum_{j=0}^{n-1} 2n+1 C_{2j+1} \hat{P}_1^{2n-2j} \rho_d^1 \hat{P}_1^{2j+1} \sum_{k=0}^{m-1} 2m C_{2k+1} \hat{P}_2^{2m-2k-1} \rho_d^2 \hat{P}_2^{2k+1} \\
& + \sum_{n=0}^{\infty} \frac{(-ig)^{2n+1}}{(2n+1)!} \sum_{m=0}^{\infty} \frac{(-ig)^{2m+1}}{(2m+1)!} \left(- \langle \psi_f | \hat{A} | \psi_i \rangle \langle \psi_i | \hat{B} | \psi_f \rangle \sum_{j=0}^n 2n+1 C_{2j} \hat{P}_1^{2n+1-2j} \rho_d^1 \hat{P}_1^{2j} \sum_{k=0}^{m-1} 2m+1 C_{2k+1} \hat{P}_2^{2m-2k} \rho_d^2 \hat{P}_2^{2k+1} \right. \\
& \left. - \langle \psi_f | \hat{B} | \psi_i \rangle \langle \psi_i | \hat{A} | \psi_f \rangle \sum_{j=0}^{n-1} 2n+1 C_{2j+1} \hat{P}_1^{2n-2j} \rho_d^1 \hat{P}_1^{2j+1} \sum_{k=0}^m 2m+1 C_{2k} \hat{P}_2^{2m+1-2k} \rho_d^2 \hat{P}_2^{2k} \right) \left. \right]. \tag{III-19}
\end{aligned}$$

As in equation (III-15), the expectation value of the joint pointer positions is obtained as

$$\langle \hat{X}_1 \hat{X}_2 \rangle' = \frac{1}{2 Tr \rho' \Pi_f} \text{Re}[\langle \psi_f | \hat{A} | \psi_i \rangle \langle \psi_i | \hat{B} | \psi_f \rangle]. \tag{III-20}$$

IV. UPPER BOUND OF S_{DFM} IN EQUATION (3)

Using equation (III-16), the S of the CHSH inequality under DFM is now expressed as

$$\begin{aligned}
S_{\text{DFM}} &= \langle \hat{A}_1 \hat{B}_1 \rangle_{\text{DFM}} + \langle \hat{A}_2 \hat{B}_1 \rangle_{\text{DFM}} + \langle \hat{A}_1 \hat{B}_2 \rangle_{\text{DFM}} - \langle \hat{A}_2 \hat{B}_2 \rangle_{\text{DFM}}, \\
&= \frac{1}{2} (\langle \hat{A}_1 \hat{B}_1 \rangle + \langle \hat{A}_1 \rangle \langle \hat{B}_1 \rangle + \langle \hat{A}_2 \hat{B}_1 \rangle + \langle \hat{A}_2 \rangle \langle \hat{B}_1 \rangle + \langle \hat{A}_1 \hat{B}_2 \rangle + \langle \hat{A}_1 \rangle \langle \hat{B}_2 \rangle - \langle \hat{A}_2 \hat{B}_2 \rangle - \langle \hat{A}_2 \rangle \langle \hat{B}_2 \rangle). \tag{IV-1}
\end{aligned}$$

Note that equation (IV-1) is rewritten as

$$S_{\text{DFM}} = \frac{1}{2} (S_I + S_{II}), \tag{IV-2}$$

with the joint average $S_I = \langle \hat{A}_1 \hat{B}_1 \rangle + \langle \hat{A}_2 \hat{B}_1 \rangle + \langle \hat{A}_1 \hat{B}_2 \rangle - \langle \hat{A}_2 \hat{B}_2 \rangle$ and the multiplication of the averages $S_{II} = \langle \hat{A}_1 \rangle \langle \hat{B}_1 \rangle + \langle \hat{A}_2 \rangle \langle \hat{B}_1 \rangle + \langle \hat{A}_1 \rangle \langle \hat{B}_2 \rangle - \langle \hat{A}_2 \rangle \langle \hat{B}_2 \rangle$.

We expect that the S_{DFM} of an arbitrary pure two-qubit state, $c_1|00\rangle + c_2|01\rangle + c_3|10\rangle + c_4|11\rangle$ ($\sum_i |c_i|^2 = 1$), is a function of the degree of entanglement. We easily estimate S_{DFM} in two extreme cases, the singlet state (one of the Bell states) and a pure separable state. For the singlet state

$$|\psi^-\rangle = \frac{1}{\sqrt{2}} (|+1\rangle - |-1\rangle), \tag{IV-3}$$

we find $S_{\text{DFM}} = \sqrt{2}$, as $S_I = 2\sqrt{2}$ and $S_{II} = 0$, because $\langle \psi^- | \vec{n} \cdot \vec{\sigma}_i | \psi^- \rangle = 0$. For a pure separable state, we obtain $S_{\text{DFM}} = 2$, as $S_I = S_{II} = 2$, because $\langle \hat{A} \hat{B} \rangle = \langle \hat{A} \rangle \langle \hat{B} \rangle$. Figure IV.1 presents the numerically calculated maximum

value of S_{DFM} and ordinary value S of CHSH inequality as a function of concurrence [2] for all possible pure states. This figure clearly shows that the upper bound of S_{DFM} for arbitrary states is equal to 2 and the decreasing value is the most dramatic for maximally entangled states.

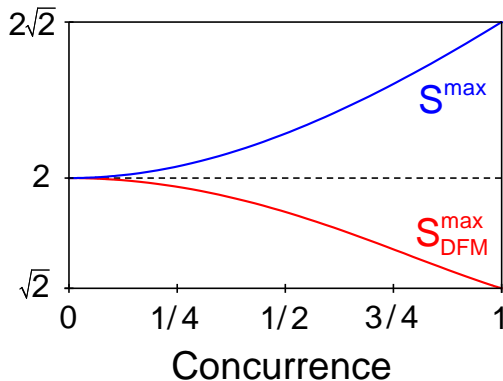


FIG. IV.1. Maximum values of S and S_{DFM} according to concurrences of pure two-qubit states. $S_{\text{DFM}}^{\text{max}}$: numerically calculated result.

V. LOCAL HIDDEN VARIABLE MODEL DESCRIBING OUR RESULTS

TABLE I. Probability distribution of all possible outcomes of CHSH test.

λ	particle 1		particle 2		$P(\lambda_i)$
	A	A'	B	B'	
λ_1	+1	+1	+1	+1	P_1
λ_2	+1	+1	+1	-1	P_2
λ_3	+1	+1	-1	+1	P_3
λ_4	+1	+1	-1	-1	P_4
λ_5	+1	-1	+1	+1	P_5
λ_6	+1	-1	+1	-1	P_6
λ_7	+1	-1	-1	+1	P_7
λ_8	+1	-1	-1	-1	P_8
λ_9	-1	+1	+1	+1	P_9
λ_{10}	-1	+1	+1	-1	P_{10}
λ_{11}	-1	+1	-1	+1	P_{11}
λ_{12}	-1	+1	-1	-1	P_{12}
λ_{13}	-1	-1	+1	+1	P_{13}
λ_{14}	-1	-1	+1	-1	P_{14}
λ_{15}	-1	-1	-1	+1	P_{15}
λ_{16}	-1	-1	-1	-1	P_{16}

Here, we present a hidden variable model describing the classical results obtained from our DFM. To test the CHSH inequality we need 4 binary observables, namely A , A' , B , and B' so that 16 hidden variables, λ_i 's and the corresponding probabilities, P_i 's, are required as shown in Table I. Then we find a set of constraints; normalization expressed as $\sum_i P_i = 1$, the averages of a single observable $\langle A \rangle_{\text{DFM}} = \langle A' \rangle_{\text{DFM}} = \langle B \rangle_{\text{DFM}} = \langle B' \rangle_{\text{DFM}} = 0$ and those of correlations $\langle AB \rangle_{\text{DFM}} = \langle A'B \rangle_{\text{DFM}} = \langle AB' \rangle_{\text{DFM}} = -\langle A'B' \rangle_{\text{DFM}} = -\sqrt{2}/4$. These constitute a system of 9 linear

equations of variable P_i 's written as

$$\begin{pmatrix} +1 & +1 & +1 & +1 & +1 & +1 & +1 & +1 & +1 & +1 & +1 & +1 & +1 & +1 & +1 \\ +1 & +1 & +1 & +1 & +1 & +1 & +1 & +1 & -1 & -1 & -1 & -1 & -1 & -1 & -1 \\ +1 & +1 & +1 & +1 & -1 & -1 & -1 & -1 & +1 & +1 & +1 & +1 & -1 & -1 & -1 \\ +1 & +1 & -1 & -1 & +1 & +1 & -1 & -1 & +1 & +1 & -1 & -1 & +1 & +1 & -1 \\ +1 & -1 & +1 & -1 & +1 & -1 & +1 & -1 & +1 & -1 & +1 & -1 & +1 & -1 & -1 \\ +1 & +1 & -1 & -1 & +1 & +1 & -1 & -1 & -1 & -1 & +1 & +1 & -1 & -1 & +1 \\ +1 & +1 & -1 & -1 & -1 & -1 & +1 & +1 & +1 & +1 & -1 & -1 & -1 & -1 & +1 \\ +1 & -1 & +1 & -1 & +1 & -1 & +1 & -1 & -1 & +1 & -1 & +1 & -1 & -1 & +1 \\ +1 & -1 & +1 & -1 & -1 & +1 & -1 & +1 & +1 & -1 & +1 & -1 & -1 & +1 & +1 \end{pmatrix} \begin{pmatrix} P_1 \\ P_2 \\ P_3 \\ P_4 \\ P_5 \\ P_6 \\ P_7 \\ P_8 \\ P_9 \\ P_{10} \\ P_{11} \\ P_{12} \\ P_{13} \\ P_{14} \\ P_{15} \\ P_{16} \end{pmatrix} = \begin{pmatrix} 1 \\ 0 \\ 0 \\ 0 \\ 0 \\ -\sqrt{2}/4 \\ -\sqrt{2}/4 \\ -\sqrt{2}/4 \\ \sqrt{2}/4 \end{pmatrix} \quad (\text{V-1})$$

Since the number of equations is smaller than that of unknowns, this is an indeterminate system so that we have infinite number of hidden variable models describing our results.

VI. LEGGETT-GARG INEQUALITY VIA MEASUREMENT WITHOUT DISTURBANCE

If two postulates, the macroscopic realism and non-invasive measurability, are established, the so-called Leggett-Garg inequality (LGI) is satisfied:

$$\langle I_{t_1} I_{t_2} \rangle + \langle I_{t_2} I_{t_3} \rangle - \langle I_{t_1} I_{t_3} \rangle \leq 1, \quad (\text{VI-1})$$

where I_{t_i} indicates a measurement outcome of the macroscopic observable I at time t_i ($t_1 < t_2 < t_3$), and these terms are dichotomic, i.e., $I_{t_i} = \pm 1$. Macroscopic realism implies that measurement of a macroscopic system reveals a well-defined pre-existing value. The postulate of non-invasive measurability states that, in principle, we can measure this value without disturbing the system. This inequality is also regarded as one form of ‘‘classicality’’, like the Bell inequality.

If we apply our disturbance-free measurement to the LGI, we trivially find that the LGI is satisfied. The correlation of two observables obtained at two distinct times can be separated as

$$\langle \hat{I}_{t_i} \hat{I}_{t_j} \rangle_{\text{DFM}} = \frac{\langle \psi_i | \hat{I}_{t_i} | \psi_i \rangle \langle \psi_i | \hat{I}_{t_j} | \psi_i \rangle}{\langle \psi_i | \psi_i \rangle \langle \psi_i | \psi_i \rangle} = \langle \hat{I}_{t_i} \rangle \langle \hat{I}_{t_j} \rangle, \quad (\text{VI-2})$$

because, in the DFM scheme, the entire procedure is completed with projection measurement for post-selection. The measurement of \hat{I}_{t_i} collapses the initial state ψ_i to the initial state itself at t_i , and we subsequently perform our DFM on \hat{I}_{t_j} with the same ψ_i at t_j ($t_i < t_j$).

VII. POLARIZATION-ENTANGLED PHOTON-PAIR SOURCE

We use a type-II non-collinear SPDC process with a PPKTP crystal ($\Lambda=10 \mu\text{m}$, $L=10 \text{mm}$) and a compensation setup to generate photon pairs having maximally entangled polarizations, with $|\phi^+\rangle = (|HH\rangle + |VV\rangle)/\sqrt{2}$ [3]. The polarization-entangled photon pairs are coupled into SMFs. For 4-mW pump power, the single counts of each port for $|H\rangle$ or $|V\rangle$ are approximately 180 kHz, and the net coincidence counts for $|HH\rangle$ and $|VV\rangle$ are 19 kHz. The polarization state (ϕ^+) is modified to the singlet state (ψ^-) via PCs and a phase controller ϕ_1 , as shown in Fig. 2. Using projection measurement (blocking one arm of the weak-measurement apparatus), we obtain polarization correlation visibilities [4] larger than 95 % and confirm the singlet state.

VIII. WEAK-MEASUREMENT SETUP ALIGNMENT

The glasses of the weak-measurement apparatus shown in Fig. 2 are used to control the beam displacement. However, the glasses also induce an optical path length difference between the two arms. To remove this difference,

we employ auxiliary setups (not shown in Fig. 2). Two linear polarizers of $\pm 45^\circ$ are temporally installed between the BDs and HWPs (denoted θ_i or $45 - \theta_i$ in Fig. 2). Using an SMF-coupled continuous-wave (cw) laser (at 810 nm) and a charge-coupled-device (CCD) camera, we measure the output-beam interference pattern. By finding the glass tilting angles that yield maximum visibility and centring the destructive interference patterns, we remove the optical path length differences. The phase between two arms is stable for a period longer than three days.

IX. PROBABILITY DISTRIBUTION MEASUREMENT VIA SMF

Usually, the probability distributions in the case of weak measurement are measured using narrow slits [5, 6]. Instead of slits, we employ couplers (collimators) with SMFs, which yields two advantages. First, this ensures that the spatial modes of the two input beams entering the NPBS in the Bell-state analyser are identical. Second, we can achieve effectively weaker measurement strength. The scanning process of SMF-to-SMF coupling ensures that the Gaussian profiles of the input beams themselves remain unchanged, with only their widths being broadened. We can redefine the beam-profile width as an effective value, such that

$$\begin{aligned} & \vec{D} G(c_1, \sigma_1) + \vec{E} G(c_2, \sigma_1) \\ \xrightarrow{*G(\sigma_2)} & \vec{D} G(c_1, \sigma_3) + \vec{E} G(c_2, \sigma_3), \end{aligned} \quad (\text{IX-1})$$

where $G(c_i, \sigma_j)$ is a Gaussian function with center position c_i and width σ_j , and $\sigma_3^2 = \sigma_1^2 + \sigma_2^2$. In this Gaussian convolution process, σ_1 is the original width of the initial beam, σ_2 is the width of the detection-component scanning coupler, and σ_3 is the effective width of the measured profiles. \vec{D} and \vec{E} represent other degrees of freedom, such as the polarizations and amplitudes. With fixed displacement $|c_2 - c_1|$ and broadened width, the strength of the weak measurement is effectively downscaled.

X. SIMULATION OF DETECTION PROBABILITY DISTRIBUTIONS

In Fig. 3b, we show simulated detection probability distributions depending on the post-selected states. These simulations can be conducted using the equations given in Sec. III. However, this approach is cumbersome, because of the excessive number of terms in these expression. Here, we show a direct calculation method for the device (pointer) state distributions after post-selection. The initial states of the system and two devices are separable, as

$$|\Psi\rangle = |\psi_s\rangle_{12} |\psi_G(x_0, \sigma)\rangle_{d_1} |\psi_G(y_0, \sigma)\rangle_{d_2}, \quad (\text{X-1})$$

where $|\psi_G(c_0, \sigma)\rangle_{d_i}$ is the device state prepared as a Gaussian with center c_0 and width σ . We assume that the initial center positions are zero and that the two device states have the same width. A weak measurement process is a translation operation T to the device state depending on the measurement basis states. Therefore, the joint weak measurement has the form

$$JWM = (|1_A\rangle_1 \langle 1_A| T_x(1) + |-1_A\rangle_1 \langle -1_A| T_x(-1)) \otimes (|1_B\rangle_2 \langle 1_B| T_y(1) + |-1_B\rangle_2 \langle -1_B| T_y(-1)), \quad (\text{X-2})$$

where $|\pm 1_M\rangle$ is the eigenstate of the measurement M with eigenvalue ± 1 . The degree of device translation corresponds to the eigenvalues. After post-selection to a final state $|\psi_f\rangle$, the wavefunction of the two devices has the form $\langle x| \langle y| \langle \psi_f| JWM |\Psi\rangle$. Therefore, the two-dimensional detection probability distribution without normalization is

$$P_{\psi_f}(x, y) = |\langle x| \langle y| \langle \psi_f| JWM |\Psi\rangle|^2. \quad (\text{X-3})$$

Note that the simulation results in Fig. 3b were calculated using equation (X-3) and effective σ , which is experimentally measured and renormalized with an experimental translation distance g .

XI. THEORETICAL VALUE OF $|S|$ DEPENDING ON POST-SELECTION

The value of $|S|$ obtained via DFM ($s \rightarrow 0$, $\langle \psi_f | \psi_i \rangle = 1$) in Fig. 4a is explained in Sec. IV. For the cases of post-selections to the ψ^+ , ψ^- states shown in Fig. 4b and c, the values of the $\langle AB \rangle$, $\langle AB' \rangle$, $\langle A'B \rangle$, and $\langle A'B' \rangle$ correlations are symmetric when the observables are chosen for $A = \hat{Z}$, $A' = \hat{X}$, $B = \frac{\hat{X} + \hat{Z}}{\sqrt{2}}$, and $B' = \frac{-\hat{X} + \hat{Z}}{\sqrt{2}}$.

Therefore, the theoretical values of $|S|$ in Fig. 4b and c are identical. As expressed in equation (III-20), the joint-observable expectation values with post-selection to the orthogonal states can diverge, because the normalization factor of equation (III-20), shown in equation (III-18), is zero when $s = 0$. Therefore, the value of $|S|$ in Fig. 4b and c diverges at $s = 0$. However, for the case of post-selection to the ϕ^+ state shown in Fig. 4d, the numerator in equation (III-20) is also zero, when the joint observables are defined as given above. Therefore, the theoretical value of $|S|$ in Fig. 4d is zero, regardless of s . At the strong measurement limit ($1 \ll s$), the correlation values converge to conditional values of sequential strong measurements. Therefore, the values of $|S|$ for strong measurement depending on four post-selections can be calculated simply.

-
- [1] K. Nakamura, A. Nishizawa, and M.-K. Fujimoto, Phys. Rev. A **85**, 012113 (2012).
 - [2] S. Hill and W. K. Wootters, Phys. Rev. Lett. **78**, 5022 (1997).
 - [3] S. M. Lee, H. Kim, M. Cha, and H. S. Moon, Opt. Express **24**, 2941 (2016).
 - [4] P. G. Kwiat, K. Mattle, H. Weinfurter, A. Zeilinger, A. V. Sergienko, and Y. Shih, Phys. Rev. Lett. **75**, 4337 (1995).
 - [5] N. W. M. Ritchie, J. G. Story, and R. G. Hulet, Phys. Rev. Lett. **66**, 1107 (1991).
 - [6] B. L. Higgins, M. S. Palsson, G. Y. Xiang, H. M. Wiseman, and G. J. Pryde, Phys. Rev. A **91**, 012113 (2015).